Eur. Phys. J. B **18**, 595–600 (2000)

THE EUROPEAN PHYSICAL JOURNAL B
EDP Sciences

de Haas-van Alphen effect and the Fermi surface of $PrNi_5$

K. Krug[1], K. Winzer[1], M. Reiffers[2,a], J. Kuneš[3], P. Novák[3], and F. Kayzel[4]

[1] I. Physikalisches Institut der Universität Göttingen, Bunsenstrasse 9, 37073 Göttingen, Germany
[2] Institute of Experimental Physics, Watsonova 47, 04353, Košice, Slovakia
[3] Institute of Physics, Academy of Sciences of the Czech Republic, Cukrovarnická 10, 162 53 Praha 6, Czech Republic
[4] Van der Waals - Zeeman Institute, University of Amsterdam, Valckenierstraat 65, 1018 XE Amsterdam, The Netherlands

Received 9 May 2000 and Received in final form 20 September 2000

Abstract. The Fermi surface of $PrNi_5$ has been studied by the measurements of the de Haas-van Alphen (dHvA) effect at temperatures between 0.3 and 1.8 K in magnetic fields up to 12 T. Two dHvA frequencies have been obtained. The electronic structure of $PrNi_5$ was calculated using the full potential linearized augmented plane wave method. Five sheets of the Fermi surface and the multiple extremal cross sections were determined. First and second sheet have a hole-like structure. The agreement between theory and experiment is obtained by a small downward shift (≈ 0.1 eV) of the Fermi energy which is probably due to an underestimation of the role of $4f$ electrons.

PACS. 71.18.+y Fermi surface: calculations and measurements; effective mass, g factor – 71.20.Lp Intermetallic compounds

1 Introduction

Intermetallic compounds $RENi_5$ (RE-rare earth) exhibit a variety of interesting physical phenomena. Among these compounds the van Vleck paramagnet $PrNi_5$ is the system which has been extensively studied. $PrNi_5$ crystallizes in the hexagonal lattice structure of the $CaCu_5$ type [1]. Although bilinear exchange interactions are present, they are under critical to induce a $4f$ magnetic order in this system because of the existence of a crystalline electric-field (CEF) singlet ground state [2,3]. Another reason of interest in $PrNi_5$ is the fact that it has been successfully used in nuclear adiabatic demagnetization experiments [2].

Previous experiments showed that all properties of $PrNi_5$ are strongly influenced by CEF. Magnetic properties are quite well understood. The influence of the quadrupolar moment on the magnetic and magnetoelastic properties enabled to determine the magnetoelastic and total quadrupolar coefficients G^α and G^ϵ, leading to the experimental evidence of antiferroquadrupolar interactions between rare-earth ions in magnetic properties [4]. The anisotropic electrical magnetoresistivity behavior of a $PrNi_5$ single crystal has given the evidence of the quadrupolar scattering of the conduction electrons [5].

Direct measurements of the anisotropic Zeeman splitting of the CEF levels, in magnetic fields up to 22 T, have been performed by point-contact spectroscopy [6]. The interpretation of the experiment led to a slight adjustment of the CEF parameters so that they account better for the position of the first excited CEF level observed by this technique in a magnetic field. The *ab initio* calculated CEF parameters of $PrNi_5$ are in a good agreement with previous experimental ones [7].

On the other hand, there is only a little information available about the electron structure of all $RENi_5$ compounds. Up to now there is no information about the Fermi surfaces and the band structure calculations [8]. Therefore, we investigated the de Haas-van Alphen (dHvA) effect in $PrNi_5$ in order to determine the Fermi surface characteristics. We present also the band structure calculations and the figures of the calculated Fermi surface.

[a] e-mail: reiffers@saske.sk

2 Experimental

A $PrNi_5$ single crystal approximately 1 cm in diameter was prepared by the Czochralski single-crystal-growth method. This single crystal was oriented by Laue diffraction for the determination of $[10\bar{1}0]$, $[12\bar{3}0]$ and [0001] directions of the hexagonal lattice (orthohexagonal definition of axis). The directions $[10\bar{1}0]$ and $[12\bar{3}0]$ are parallel to the basal plane and [0001] is perpendicular to the basal plane of the hexagonal lattice. After the orientation of single crystal we prepared by spark-cutting three cylindrical samples (called #1, #2 and #3), with cylinder axis parallel to $[10\bar{1}0]$, $[12\bar{3}0]$ and [0001], respectively. For the sample purity characterization the residual resistivity ratio $RRR \equiv \rho(300\ \mathrm{K})/\rho(4.2\ \mathrm{K})$ was determined in four point geometry with lock-in technique.

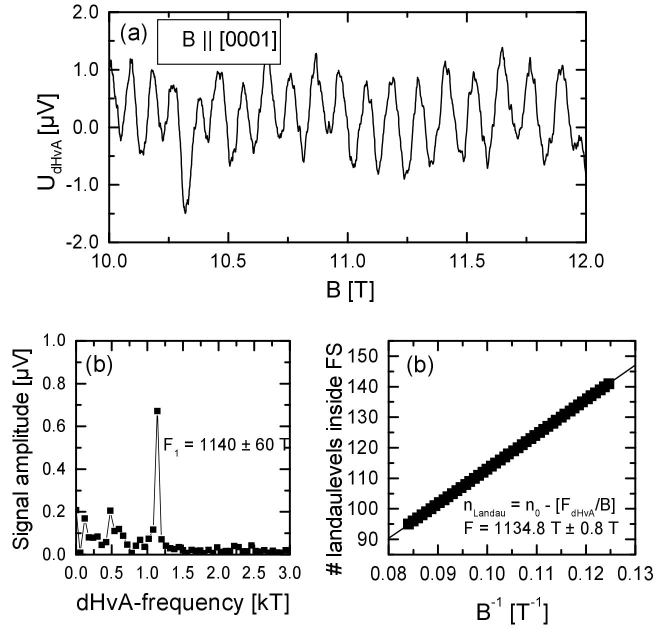

Fig. 1. (a) Oscillating dHvA signal and (b) determination of its corresponding frequency at 0.6 K between 10 and 12 T for $B||[0001]$ in sample #3.

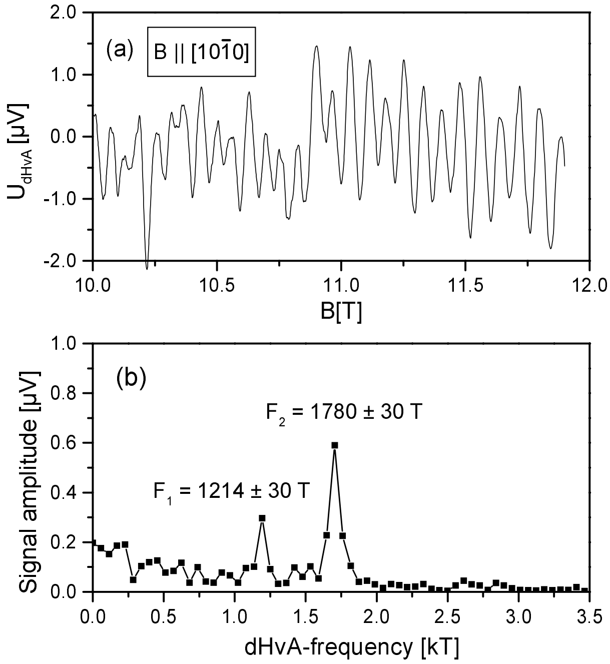

Fig. 2. (a) Oscillating dHvA signal and (b) determination of its corresponding frequency at 0.6 K between 10 and 12 T for $B||[10\bar{1}0]$ in sample #1.

From these measurements we have estimated the RRR-values which are largest for the $[10\bar{1}0]$ orientated sample with $RRR \approx 17$ and smaller ($RRR \approx 10$) for the other ones. Since we need as pure as possible single crystals for the dHvA-measurements we expected better conditions for sample #1 than for the others. The cylindrical samples were mounted inside a compensated coil system where the oscillating dHvA-signal was measured inductively in the magnetic field up to 12 T. In this way the samples induce an oscillating voltage as a function of the reciprocal field due to the oscillating part of their susceptibility [9]. To determine angular dependences of the dHvA-frequencies the coil system with the sample could be rotated with respect to the magnetic field direction.

3 Experimental results

For three samples with cylinder axis parallel to $[10\bar{1}0]$, $[12\bar{3}0]$ and $[0001]$ we measured two different dHvA-frequencies, their angular dependence for tilting angles $\alpha \leq 40°$ of the cylinder axis with respect to the magnetic field and one effective mass belonging to the smaller one of the two frequencies. Figure 1a shows the measured dHvA-oscillations on sample #3 with the magnetic field B parallel to the $[0001]$ sample direction. Since in this direction only one frequency is clearly visible, the frequency can be determined by usual fast Fourier transformation (FFT) and additionally by the slope of a so-called Landau plot, where the position of each periodic repeating signal value, for instance maxima and minima, is plotted against the reciprocal field (Fig. 1b). For the increasing field in each period one Landau cylinder has left the Fermi surface. These analyses result in one dHvA frequency of $F_1 = 1.13$ kT equal to a Fermi surface cross section of $S_1 = F_1(2\pi e)/\hbar = 10.8\ \text{nm}^{-2}$. This frequency could be detected with a nearly isotropic value in all three samples. Its detailed angular dependence is shown in Figure 12a. Figure 2a shows the measured dHvA-oscillations on sample #1 and the corresponding FFT spectrum (Fig. 2b). The FFT of the signal results in two frequencies with $F_1 \approx 1.2$ kT and $F_2 \approx 1.78$ kT which are equal to cross sections $S_1 \approx 10.8\ \text{nm}^{-2}$ and $S_2 \approx 17.0\ \text{nm}^{-2}$. Again the detailed angular dependence of the frequencies is shown in Figure 12b. In the range of angles α between B and the $[10\bar{1}0]$-direction where the oscillations were observable, *e.g.* $\alpha \equiv \angle(B, [10\bar{1}0]) \leq 40°$, the frequency F_2 increases monotonically while F_1 remains rather constant.

The amplitude of a dHvA signal for one frequency depends on temperature as [9]

$$R_T = \frac{x}{\sinh(x)} \quad \text{with } x = 14.693\ \text{T/K} \frac{m_c}{m_0} \frac{T}{\bar{B}} \qquad (1)$$

where m_0 is the free electron mass and m_c denotes the cyclotron mass of the electrons in the extremal orbit corresponding to the observed frequency, while T and $\bar{B}$ are the temperature and average field of one dHvA-experiment. For sample #3 we performed dHvA-measurements at fixed orientation $B||[0001]$, equal field ranges $\bar{B}$ but at different constant temperatures $T \leq 1.2$ K and we estimated dHvA-amplitudes. In Figure 3 we plotted the amplitudes of each measurement against the temperature. By fitting of these values by equation (1) one obtains the cyclotron mass as a fitting parameter under the boundary condition $R_T(T = 0\ \text{K}) \equiv 1$. In this way the corresponding effective mass of frequency F_1 is estimated as $m_c = 1.43\, m_0$. This corresponds to a Fermi velocity $v_F = \sqrt{2\, e\, \hbar F_1}/m_{c_1} = 1.5 \times 10^7\ \text{cm}\,\text{s}^{-1}$. The effective mass of the electrons also

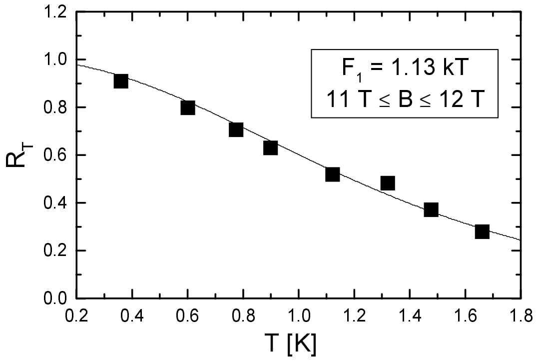

Fig. 3. Temperature dependence of the dHvA-signal corresponding to F_1 below 1.8 K. The squares are from experiments and the line is the fitting result of equation (1).

enters the sample quality dependent amplitude factor, called Dingle factor R_{D} [9]

$$R_{\mathrm{D}} = \exp\left(-14.693\ \mathrm{T/K}\frac{m_{\mathrm{c}}}{m_0}\frac{T_{\mathrm{D}}}{B}\right). \qquad (2)$$

Here T_{D} describes the sample purity in dimensions of a temperature, where larger temperatures belong to worse sample quality. It follows from equation (2), that frequencies with large effective masses are hardly detectable in imperfect samples. Moreover, it follows that larger effective masses normally belong to larger frequencies, since the Fermi velocities of different orbits are rather constant. Taking this estimation and equation (2) into account, the worse sample quality of #2 and #3 and the probably larger effective mass of F_2 might be the reason why frequency F_2 is only detectable in our best sample #1.

4 Calculation of the Fermi surface

The full potential linearized augmented-plane-waves (FLAPW) code WIEN97 [10] was used for band structure calculation in order to determine the Fermi surface. The electronic states are divided into several groups within the present implementation of FLAPW method:

- valence states (5*d*, 6*s*, 6*p* states of Pr; 3*d*, 4*s*, 4*p* states of Ni),
- local orbitals [11] (5*s* and 5*p* states of Pr; 3*p* states of Ni),
- core states, which in our case comprise remaining electronic states of both Pr and Ni except the 4*f* states of Pr,
- 4*f* states of Pr. Because of their strong correlation and charge inhomogeneity the 4*f* electrons are not correctly described by the band calculation. For this reason we treat them as a separate group of semicore levels for which the hybridization with the valence states, as well as the dispersion, are prevented [7]. This approach is equivalent to the 'open core' treatment of the 4*f* states [12]. The number of 4*f* electrons was assumed to be two, corresponding to the 3+ valence state of praseodymium.

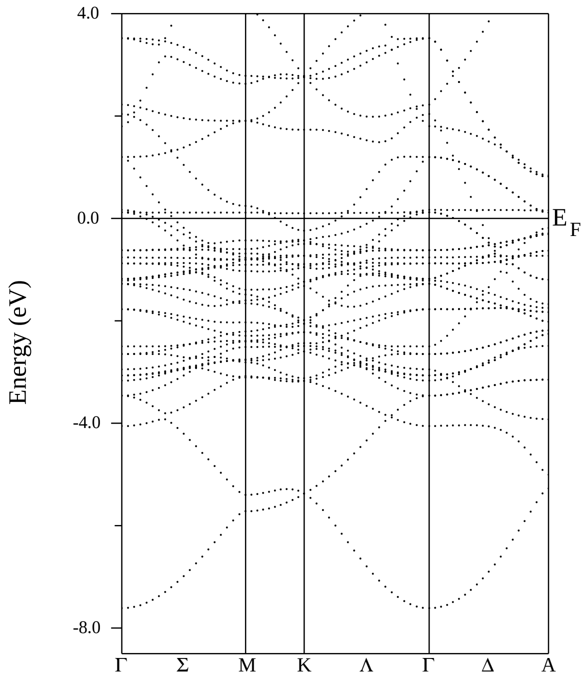

Fig. 4. Valence electron's bandstructure of $PrNi_5$.

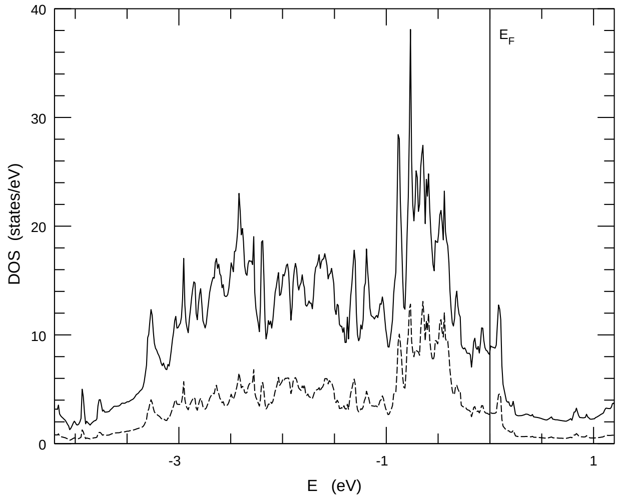

Fig. 5. Density of states of $PrNi_5$ (full curve) and sum of the partial densities of *d*-states of Ni(I) and Ni(II) (dashed curve).

The calculations reported here were non spin-polarized, performed for experimental values of the $PrNi_5$ lattice constant on 133 *k*-points in the irreducible wedge of the Brillouin zone. LDA exchange-correlation potential (Perdew and Wang [13] reparametrization of Ceperley and Alder data) was used. Atomic sphere radii were 3.208 a.u. and 2.2 a.u. for Pr and Ni, respectively. The resulting band structure along the symmetry directions is shown in Figure 4. There are five bands intersecting the Fermi level resulting in five sheets of the Fermi surface (only four bands crossing the Fermi level are visible in Fig. 4 since the fifth sheet lies off all the high symmetry directions). The dominant contribution to the density of states in the vicinity of Fermi energy comes from the 3*d* states of Ni as seen from Figure 5.

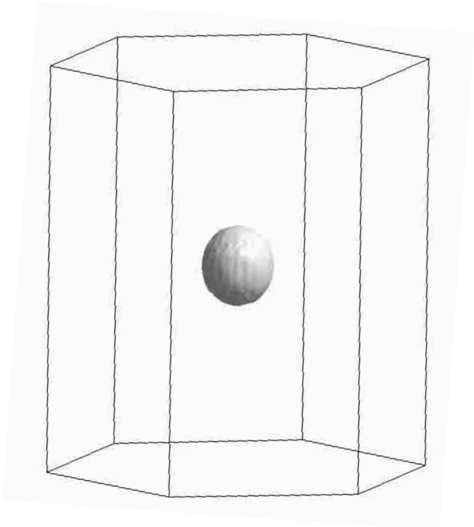

Fig. 6. Fermi surface of first conduction band.

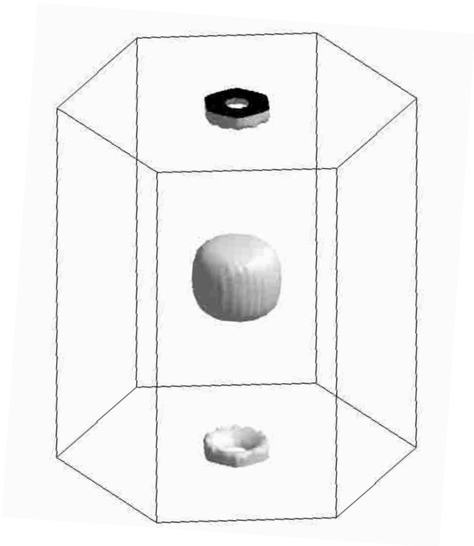

Fig. 7. Fermi surface of second conduction band.

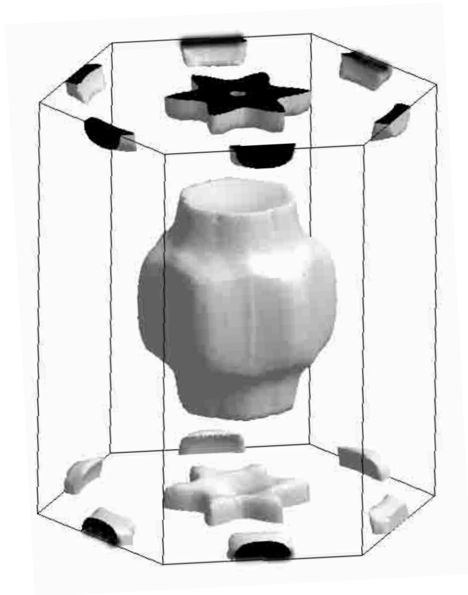

Fig. 8. Fermi surface of third conduction band.

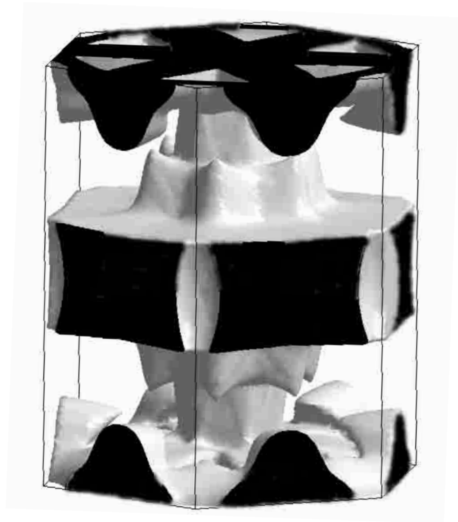

Fig. 9. Fermi surface of fourth conduction band.

The potentials obtained in the selfconsistent calculation were used to calculate the eigenenergies on a very dense k-point mesh (35 301 points in the irreducible wedge of the Brillouin zone). The four point interpolation was then used to find the Fermi vectors k_F. The calculated sheets of the Fermi surface are shown in Figures 6–10.

First and second sheets are hole-like surfaces. First sheet has a spherical shape. Second sheet consists of two parts: a slightly irregular ellipsoid in the center of the Brillouin zone and a ring at the zone boundary. Third sheet consists of vase-like electron surface in the zone center, stars and small bone-like electron pockets at the zone boundary. Fourth sheet is a complicated open surface of a layers-and-columns shape. Fifth sheet consists of electron surface of an irregular ring shape and small electron pockets at the zone boundary.

Only two dHvA-frequencies were observed experimentally. This is most probably connected with the insufficient purity of the sample and the field limitation of 12 T. In order to assign the experimental dHvA-frequencies to their theoretical counterparts, first we have analyzed the shape of the Fermi surface in relation to the dHvA-frequency *vs.* magnetic field orientation data. We have concluded that except the central parts of sheets 1, 2 and 3, all pockets of the Fermi surface will generate a dHvA-frequency rapidly changing with magnetic field tilted out of the hexagonal axis direction. For the three candidates (sheets 1, 2 and 3) we calculated the dHvA-frequency *vs.* magnetic field orientation dependences (Fig. 11).

Comparing the theoretical dependences with the experimental data we could identify the lower branch with first sheet and the upper branch with the central part of second sheet of the Fermi surface. However, the calculated values of dHvA frequencies are smaller by a factor of approximately 1.5 compared with the experimental values. As can be seen from Figure 4 a downward shift

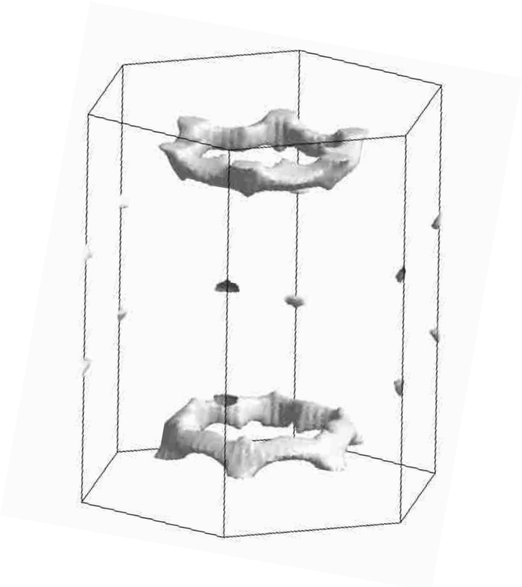

Fig. 10. Fermi surface of fifth conduction band.

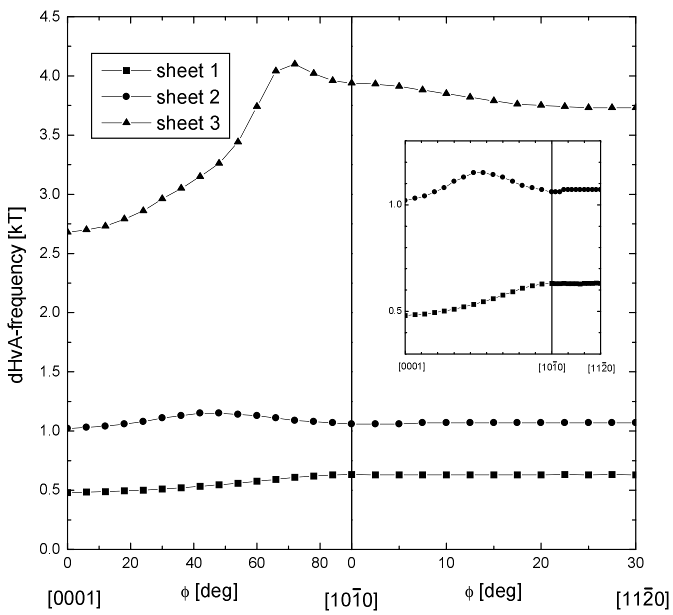

Fig. 11. Calculated dHvA-frequencies corresponding to first sheet and the central pockets of second and third sheets of the Fermi surface as a function of the magnetic field orientation. The branches corresponding to first and second sheets are shown in detail in the inset.

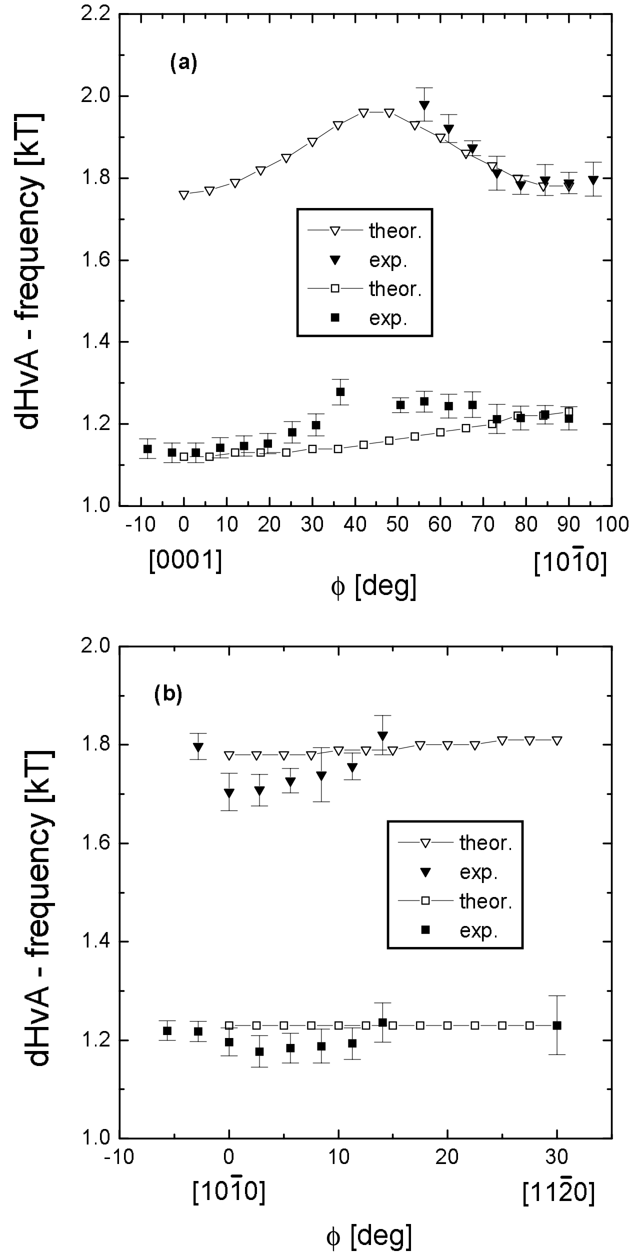

Fig. 12. Comparison of the experimental and calculated de Haas-van Alphen frequencies of the lowest two sheets of Fermi surface of $PrNi_5$ for shifted Fermi energy (0.1 eV).

of the Fermi energy E_F of approximately 0.1 eV could remove this discrepancy and we have obtained quite good agreement (Fig. 12). A similar small shift of the Fermi energy has been reported in [14] where it was obtained by a small shift of unoccupied La-4f-bands of $LaAl_2$.

The calculated band masses are: sheet 1 - $m_{b1} = 0.20m_0$; sheet 2 - $m_{b2} = 0.26m_0$ and sheet 3 - $m_{b3} = 0.34m_0$. It should be noted that the calculated band mass of the first conduction band $m_{b1} = 0.20m_0$ is very small compared to the experimentally obtained cyclotron mass $m_{c1} = 1.43m_0$. Such a strong enhancement of m_c compared to m_{b1} cannot be explained by the electron-phonon interaction only. Therefore, another enhancement mechanism must be responsible for the increase of the cyclotron mass with respect to the band mass. A possible explanation is the existence of magnetic excitons discussed in [15] in connection with the thermal conductivity of $PrNi_5$.

To see how stable the results for the Fermi surface are, two calculations with exchange-correlation potentials of Perdew and Wang [13] and Perdew *et al.* [16] were performed. The change of the first and the second sheets of the Fermi surface is small, corresponding to a change of the dHvA frequencies being less than 5%.

At present we are not able to obtain better agreement between the theory and experiment. Improvements going behind the semicore model of $4f$ electrons are necessary.

5 Conclusions

In conclusion we have examined the Fermi surface of the van Vleck paramagnet $PrNi_5$. The measurements of the de Haas-van Alphen effect have revealed two frequencies. We have performed the band structure calculations by FLAPW method and we have calculated the Fermi surface of $PrNi_5$. We are able to obtain an agreement between the theory and experiment only if we perform the downward shift of the Fermi energy at about ≈ 0.1 eV. At present, the improvements of model taking into account the possible hybridization effects and a more correct description of the role of $4f$ electrons, are necessary.

This work was supported by the grant A1010715 of the Grant Agency of AV ČR; by the grant 2/7022/20 of the Slovak grant agency VEGA and by the grant of DAAD (for M. R.). The support of the Deutsche Forschungsgemeinschaft is gratefully acknowledged. We are grateful to Tone Kokalj (Jozef Stefan Institute, Lubljana, Slovenia) for providing and helping us to use the program XCrysDen, with which the Fermi surfaces were drawn.

References

1. J.H. Wernick, S. Geller, Acta Crystall. **12**, 662 (1959).
2. K. Andres, S. Darack, Physica B **86-88**, 1071 (1977).
3. K. Andres, S. Darack, S. Ott, Phys. Rev. B **19**, 5475 (1979).
4. V.M.T.S. Barthem, D. Gignoux, A. Nait-Saida, D. Schmitt, G. Creuzet, Phys. Rev. B **37**, 1733 (1988).
5. J. Blanco, M. Reiffers, D. Gignoux, D. Schmitt, A.G.M. Jansen, Phys. Rev. B **44**, 9325 (1991).
6. M. Reiffers, Yu.G. Naidyuk, A.G.M. Jansen, P. Wyder, I.K. Yanson, D. Gignoux, D. Schmitt, Phys. Rev. Lett. **62**, 1560 (1989).
7. P. Novák, J. Kuriplach, Phys. Rev. B **50**, 2085 (1994).
8. Y. Onuki, A. Hasegawa, *Handbook of the Physics and Chemistry of Rare Earth*, edited by K.A. Gschneidner Jr, L. Eyring (Elsevier, 1995), Vol. 20, Chap. 135.
9. See for example D. Shoenberg, *Magnetic Oscillations in Metals* (Cambridge University Press, 1984).
10. P. Blaha, K. Schwarz, J. Luitz, *WIEN 97, A Full Potential Linearized Augmented Plane Wave Package for Calculating Crystal Properties* (Karlheinz Schwarz, Techn. Universität Wien, Austria, 1999).
11. D.J. Singh, *Planewaves, Pseudopotentials and the LAPW Method* (Kluwer Academic Publishers, Boston, Dordrecht, London, 1994).
12. For review of the band structure theory of $3d$-$4f$ compounds see M. Richter, J. Phys. D **31**, 1017 (1998).
13. J.P. Perdew, Y. Wang, Phys. Rev. B **45**, 13244 (1992).
14. K. Betsuyaku, H. Harima, J. Magn. Magn. Mater. (to be published, 2001).
15. M. Reiffers, K. Flachbart, A.B. Beznosov, Physica B & C **126**, 1087 (1984).
16. J.P. Perdew, S. Burke, M. Ernzzerhof, Phys. Rev. Lett. **77**, 3865 (1996).